An insight into the charge carriers transport properties and electric field distribution of CH 3 NH 3 PbBr 3 thick single crystals

Oriane Baussens, Loli Maturana, Smaïl Amari, Julien Zaccaro, Jean-Marie Verilhac, Lionel Hirsch, Eric Gros-Daillon

AUTHOR QUERY FORM

AIP Publishing	**Journal: Appl. Phys. Lett.** **Article Number: APL20-AR-03618**	**Please provide your responses and any corrections by annotating this PDF and uploading it to AIP's eProof website as detailed in the Welcome email.**

Dear Author,

Below are the queries associated with your article; please answer all of these queries before sending the proof back to AIP.

Article checklist: In order to ensure greater accuracy, please check the following and make all necessary corrections before returning your proof.

1. Is the title of your article accurate and spelled correctly?
2. Please check affiliations including spelling, completeness, and correct linking to authors.
3. Did you remember to include acknowledgment of funding, if required, and is it accurate?

Location in article	Query / Remark: click on the Q link to navigate to the appropriate spot in the proof. There, insert your comments as a PDF annotation.
AQ1	Please check that the author names are in the proper order and spelled correctly. Also, please ensure that each author's given and surnames have been correctly identified (given names are highlighted in red and surnames appear in blue).
AQ2	Please check and confirm presentation of affiliation 3.
AQ3	Please provide complete details for Ref. 2.
AQ4	Please provide volume and page number for Ref. 4.
AQ5	Please provide publisher name for Ref. 13.
AQ6	Please provide book title for Ref. 14.
	Please confirm ORCIDs are accurate. If you wish to add an ORCID for any author that does not have one, you may do so now. For more information on ORCID, see https://orcid.org/. Oriane Baussens - 0000-0003-0042-2855 Loli Maturana - 0000-0002-4324-123X Smaïl Amari - 0000-0002-5565-9481 Julien Zaccaro- Jean-Marie Verilhac- Lionel Hirsch - 0000-0003-2325-5535 Eric Gros-DAillon - 0000-0002-4196-7854
	Please check and confirm the Funder(s) and Grant Reference Number(s) provided with your submission: Horizon 2020 Framework Programme, Award/Contract Number 777222 Please add any additional funding sources not stated above:

Thank you for your assistance.

J_ID: APPLAB DOI: 10.1063/5.0011713 Date: 23-July-20 Stage: Page: 1 Total Pages: 5

PROOF COPY [APL20-AR-03618]

Applied Physics Letters ARTICLE scitation.org/journal/apl

An insight into the charge carriers transport properties and electric field distribution of $CH_3NH_3PbBr_3$ thick single crystals

Cite as: Appl. Phys. Lett. **117**, 000000 (2020); doi: 10.1063/5.0011713
Submitted: 30 April 2020 · Accepted: 30 June 2020 ·
Published Online: 0 Month 0000

Oriane Baussens,[1,a)] Loli Maturana,[1] Smaïl Amari,[2] Julien Zaccaro,[3] Jean-Marie Verilhac,[2] Lionel Hirsch,[4] and Eric Gros-DAillon[1,a)]

AFFILIATIONS

[1]University Grenoble Alpes, CEA, LETI, F38000 Grenoble, France
[2]University Grenoble Alpes, CEA, LITEN, F38000 Grenoble, France
[3]University Grenoble Alpes, CNRS, Grenoble INP, Institut Néel, BP166, 38042 Grenoble, Cedex 09, France
[4]University Bordeaux, IMS-CNRS, UMR 5218, Bordeaux INP, ENSCBP, F33405 Talence, France

[a)]**Authors to whom correspondence should be addressed:** oriane.baussens@cea.fr and eric.grosdaillon@cea.fr

ABSTRACT

Thanks to their unique combination of semiconducting properties and a large cross section for energetic photons, metal halide perovskites could theoretically achieve high x-ray to charge carriers conversion rates, making them materials of high interest for the direct x-ray detection. In this work, we focus on the transport properties of methylammonium lead tribromide ($MAPbBr_3$) single crystals. Time of Flight measurements and x-ray focused experiments along the edge of the samples were carried out. We report homogenous holes transit throughout the thickness of the samples as well as poor electrons transit. We also report the continuity of the electric field throughout the thickness of the $MAPbBr_3$ samples, and we present preliminary fitting results to discuss its nature.

Semiconducting metal halide perovskites have gained a lot of interest for solar cells applications. In the last decade, the reported efficiency perovskite based solar cells has increased from 3.81% to 25.2%.[1,2] However, the main concern for such mainstream application, as mentioned by Li *et al.*, is the presence of heavy metals in the ionic crystal.[3] On the other hand, heavy atoms like lead have large x-rays cross sections. Therefore, heavy metal halide perovskites could be perfectly suited for confined applications such as direct x-ray detectors for medical imaging. In addition to the cross section, efficient x-ray detection also requires good charge carriers' transport properties in order to optimize charge collection and reduce ghosting effect.

In this work, we investigated the photocarriers' transport properties of thick methylammonium lead tribromide ($MAPbBr_3$) single crystals. We studied the electron and hole mobilities with laser Time of Flight. The continuity of the electric field throughout the thickness of the samples was then tested by x-ray focused experiments, the first to be reported to our knowledge.

Several $MAPbBr_3$ single crystals of controlled quality were grown individually by a seeded Inverse Temperature Crystallization method. The growth procedure and crystal quality are detailed in a previous publication by Amari *et al.*.[4] The obtained single crystals had a typical size of 4 mm × 4 mm × 2 mm. Their top and bottom (100) faces were optically polished (roughness below 30 nm r.m.s), and chromium electrodes were thermally evaporated on both sides (100 nm on one side, 30 nm on the other to ensure semi-transparency). Six samples were prepared in that way, and their individual properties and $I–V_{dark}$ curves can be found in Figs. S1 and S2 of the supplementary material.

Time of Flight (ToF) is widely used to measure the mobility of carriers in semiconductors. Published ToF mobility values of $MAPbBr_3$ single crystals range from 14 to 217 $cm^2\,V\,s^{-1}$ for holes and 25–190 $cm^2\,V^{-1}\,s^{-1}$ for electrons.[5–12] When conducting ToF experiments (Fig. 1), the mobility is deduced from the transit time (t_t) of the charge carriers. In laser ToF, the carriers are photogenerated by a laser pulse in the immediate vicinity of a semi-transparent electrode: the incident wavelength is selected so as to be absorbed at depths negligible when compared to the thickness of the sample. That way, only one type of charge carriers contributes to the photocurrent by transiting through the thickness (L) of the sample to reach the opposite electrode. For a sample biased at voltage V with no trapping mechanism and a homogenous electric field, the drift mobility μ is defined as

J_ID: APPLAB DOI: 10.1063/5.0011713 Date: 23-July-20 Stage: Page: 2 Total Pages: 5

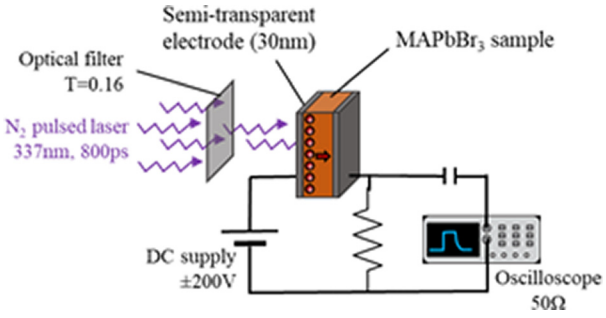

FIG. 1. Laser ToF experiment in a hole measurement configuration.

$$\mu = L^2/(V \times t_t)\,(\mathrm{cm}^2 \cdot \mathrm{V}^{-1} \cdot \mathrm{s}^{-1}). \quad (1)$$

In ToF experiments, because a large number of charge carriers are created in a narrow volume ($\approx 10^{-2}\,\mathrm{cm}^3$) near the irradiated electrode, the concentration of charges can lead to a drastic drop of the internal electric field that would reduce the transit time measured. To probe this point, the ToF photocurrent for holes for different amounts of photocarriers generated (estimation of which can be found in page 2 of the supplementary material) was measured. To that end, the incident laser intensity was varied using optical filters with transmittance (T) between 0.1 and 0.5. From the resulting photocurrent transit curves presented in Fig. 2, three observations can be made. First, the transit time of holes in sample 1 ($t_{t\text{-}h+} \sim 7.5\,\mu s$) does not depend on the light intensity for the range of fluxes used. This ensures that under our experimental conditions the photocarriers created by the laser do not perturb the internal electric field. Second, the photocurrent increases from anode to cathode independently of the transmittance (see normalized Fig. S3). Knowing that the instantaneous mobility establishes a link between the photocurrent and the position of the photocarriers at every moment in time, we can attribute the increase in the photocurrent to an increase in the internal electric field from anode to cathode. A more detailed discussion on the nature of the electric field is presented in the x-ray focused experimental section and in the supplementary material. Third, there is a sharp peak at the beginning of the photocurrent. It was attributed it to fast trapping mechanisms in a previous publication.[13]

So, in agreement with these first observations, to characterize the charge carriers mobility, we illuminated our samples with 800 ps pulses from a nitrogen laser (337 nm), using the optical filter with a transmittance of 0.16. Results for our six samples are detailed in the supplementary material (Fig. S4 for holes and Fig. S5 for electrons). Figure 3(a) shows the hole transit photocurrent of sample 1 polarized between −60 V and −140 V. The inflection indicating hole collection at the cathode is clearly visible, and the longest transit time measured is 13 μs. This value corresponds to a minimum value of the holes' lifetime in our experimental conditions. Holes' mobility measurements were reproducible among our six samples of the same crystal quality with an average of $13\,\mathrm{cm}^2\,\mathrm{V}^{-1}\,\mathrm{s}^{-1} \pm 2\,\mathrm{cm}^2\,\mathrm{V}^{-1}\,\mathrm{s}^{-1}$. Figure 3(b) shows the electron transit photocurrent of sample 1 for bias voltages between +100 V and +140 V. Electrons' mobility could not be measured satisfactorily, because the inflection of the transit photocurrent was not visible even in a log–log representation (Fig. S6). This indicates that the mobility lifetime product of electrons ($\mu_{e\text{-}}\tau_{e\text{-}}$) is not large enough to allow all the electrons to fully transit even at polarization fields as high as $1500\,\mathrm{V\,cm}^{-1}$. To estimate a maximal value for the electrons' lifetime, a Ramo's model was used [Eq. (2)]:

$$i(t) = n\,e\,\mu\,V \times \exp\left(-\frac{t}{\tau}\right)/L^2. \quad (2)$$

In this equation, n is the number of photocarriers created, e is the elementary charge, μ is the charge carrier mobility, V is the bias voltage, L is the thickness of the sample, and τ is the charge carrier lifetime. Using Eq. (2) and our experimental conditions, we tried to fit the measured photocurrent for different electron lifetimes. For lifetimes above 1.25 μs, it was impossible to model the experimental data regardless of the mobility and the bias voltage used. Therefore, we hypothesize that in our experimental conditions the electron lifetime is smaller than 1.25 μs. The inset of Fig. 3(b) displays the electron photocurrent at +140 V and the corresponding Ramo model for a lifetime of 1.25 μs.

For the case at hand, we conclude that $\mu_{e\text{-}}\tau_{e\text{-}} \ll \mu_{h+}\tau_{h+}$. This conclusion as implications on the commonly used Hecht fittings, which we discuss in the supplementary material (Fig. S7).

Using ToF experiments, a non-homogenous, anode to cathode increasing electric field was hypothesized. However, because ToF measurements are not spatially resolved, the continuity of the electric field in the volume and the position of the cathode are not assured. Therefore, additional x-ray focused experiments were conducted (Fig. 4) to verify the continuity and homogeneity of the electric field. They consist in scanning the thickness of a sample with an x-ray beam limited by 100 μm slit. The irradiation starts at one edge of the

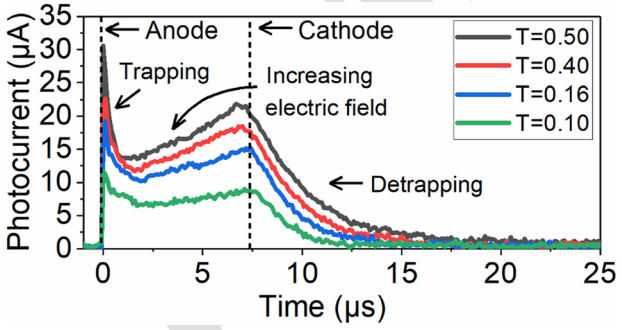

FIG. 2. Hole transit photocurrent of sample 1 biased at −100 V as a function of the transmittance of the optical filter.

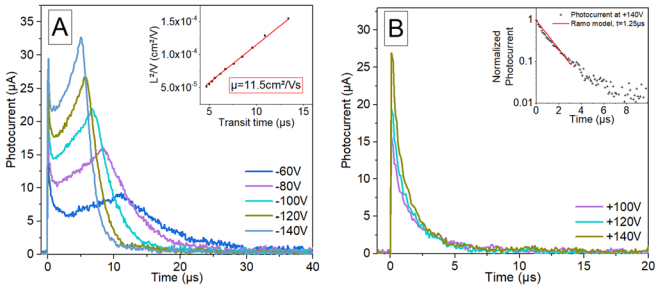

FIG. 3. (a) ToF hole photocurrent of a MAPbBr3 sample (inset: mobility calculation). (b) ToF electron photocurrent of a MAPbBr3 sample (inset: photocurrent at +140 V and Ramo model for $\tau_{e\text{-}} = 1.25\,\mu s$).

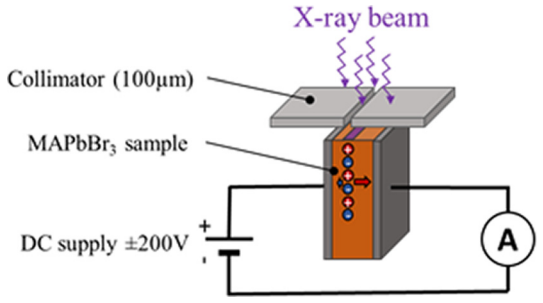

FIG. 4. X-ray focused experiment setup.

sample and moves along the thickness by 100 μm steps increments until it reaches the opposite edge. Because of the slit's width, only the samples thicker than 0.8 mm were tested. At each step, the sample is irradiated by ten pulses of x-rays generated by a varian tube using the characteristic medical radiography setups (Table I) as described in IEC 62220 International Standard.[14] The x-ray pulses were recorded via a Keithley 428 picoammeter. The experiment was reproduced using different bias voltages. For each sample and each bias voltage, the average photocurrent density was plotted as a function of the position of the irradiation along the thickness of the sample.

It is worth noting that the measurement duration (100 ms) is five orders of magnitude higher than the characteristic ToF measurement duration. This allows us to probe both the photocarriers transit and the effect of long irradiation times used in medical imaging applications. It can also be noted that the number photocarriers generated ($\approx 10^{10}$, supplementary material page 5) is smaller, and the volume in which they are generated is larger ($\approx 10^{-1}$ cm^3) than in the ToF experiments. This justifies the non-perturbation of the electric field by the photocarriers generated in the x-ray focused experiments.

Figure 5 shows the results for sample 1, those for all the other samples tested are available in the supplementary material (Fig. S8).

The photocurrent density of sample 1 is linear for all voltages and decreases as the charges are generated closer the cathode.

The experimental results may be modeled by expressing the drift photocurrent measured in x-ray focused experiment for our cuboid sample with planar electrodes [Eq. (3)]. The photocurrent is then defined as the sum of the charges induced on the electrodes by the Ramo intensity of each type of photocarriers over the duration of the measurement

TABLE I. X-ray tube setups.

Tube voltage	70 kVp
X-ray minimum energy	50 keV
Tube current	100 mA
Filtration	0.8 mm Be, 23 mm Al
Work distance	1 m
Pulse width	100 ms
Pulse frequency	4 Hz

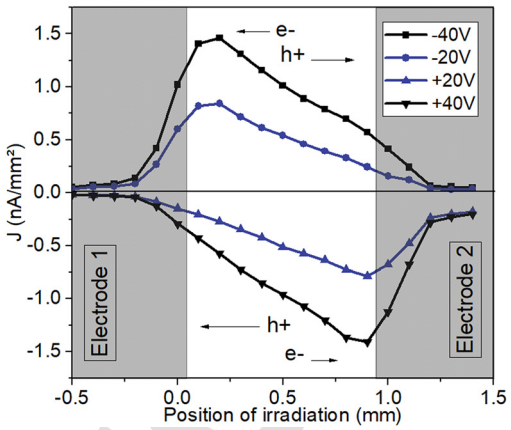

FIG. 5. Photocurrent density as a function of the position of the irradiation.

$$I_{mes}(X) = \frac{1}{t_{mes}} \times \left[\int n_{e_-}(x(t)) \exp\left(\frac{-t}{\tau_{e_-}}\right) \times \frac{e\mu_{e_-} E(x(t))}{L} dt + \int n_{h_+}(x(t)) \exp\left(\frac{-t}{\tau_{h_+}}\right) \times \frac{e\mu_{h_+} E(x(t))}{L} dt \right], \quad (3)$$

where X is the irradiation position, t_{mes} is the measurement time, n is the number of charge carriers created, $x(t)$ is the instantaneous position of the charge carriers, τ is the charge carrier lifetimes, e is the elementary charge, μ is the charge carrier mobilities, E is the electric field, and L is the thickness of the sample.

Equation (3) shows that the photocurrent depends on both the photocarriers' transport properties and the electric field distribution along the thickness of the sample. With the ToF measurements, we have established that the charge carriers' transport properties are dissymmetric ($\mu_{e\text{-}}\tau_{e\text{-}} \ll \mu_{h+}\tau_{h+}$). If we hypothesize a constant electric field, we expect to see a maximum of the photocurrent when the material is irradiated near the anode and a minimum when it is irradiated near the cathode. This is indeed what is observed on the photocurrent profiles displayed in Figs. 5 and S8.

Here, electrode 1 is grounded while electrode 2 is biased. In the case of charge creation near the anode (positive bias), the electrons are collected almost immediately while the holes transit through the entire thickness of the sample and account for most of the photocurrent measured. In the case of charge creation near the cathode (negative bias), the holes are collected almost immediately and, since the electrons cannot transit through the entire thickness of the sample (as demonstrated by the ToF experiments), the charge induced at the electrode is lower than in the previous case.

In Fig. 5, it can also be observed that the photocurrent has non-zero continuous values throughout the sample indicating a continuous and non-null electric field.

In the discussion above, a constant electric field was hypothesized to explain the shape of the photocurrent. However, the ToF data in Fig. 2 have shown that a linear field, increasing from anode to cathode is more likely. To get a better idea of the shape of the electric field, Eq. (3) was used to model the x-ray focused and ToF experimental results of sample 1 in the case of a constant electric field and a linear electric field, increasing from anode to cathode (Figs. S9 and S10).

We found that the x-ray focused experimental data could be modeled by either of those fields. However, only the linear electric field allowed modeling the ToF experimental data. This is in contradiction with the homogenous electric field hypothesis of Eq. (1). Nonetheless, the use of a constant electric field to model our data only leads to a 5% underestimation of the mobility, which is negligible compared to the 15% measurement uncertainty. More in depth modeling is under progress to achieve better fitting for both types of experimental data.

In conclusion, we have measured reproducible hole mobility of $MAPbBr_3$ single crystals of controlled quality with laser ToF at 13 $cm^2 V^{-1} s^{-1} \pm 2\ cm^2 V^{-1} s^{-1}$. We have also seen that both ToF and x-ray focused results are consistent with poor electrons' transport properties in $MAPbBr_3$ single crystals. We can only hypothesize that the lack of electrons transit is due to either deep trapping levels or recombination centers, as shown by Musiienko *et al.*[9] In the case of a deep trapping level, the detrapping constant would be higher than 100 ms, our typical measurement duration. Finally, we have shown that the internal electric field exists throughout the thickness of the samples, and our preliminary modeling results point toward it being linear and increasing from anode to cathode. Knowing the nature of the electric field is essential and will therefore be the topic of follow-up studies.

See the supplementary material for detailed samples properties, ToF and x-ray focused measurements of samples 1–6, discussion about Hecht fitting, and discussion about the constant electric field hypothesis.

The authors thank Trixell and the ATTRACT project, from the European Horizon H2020 (Grant No. 777222, PerXi project), for the financial support.

DATA AVAILABILITY

The data that support the finding of this study are available from the corresponding authors upon reasonable request.

REFERENCES

[1]A. Kojima, K. Teshima, Y. Shirai, and T. Miyasaka, "Organometal halide perovskites as visible-light sensitizers for photovoltaic cells," J. Am. Chem. Soc. **131**(17), 6050–6051 (2009).

[2]NREL. Best Research Cell Efficiency ■.

[3]J. Li, H.-L. Cao, W.-B. Jiao, Q. Wang, M. Wei, I. Cantone, J. Lü, and A. Abate, "Biological impact of lead from halide perovskites reveals the risk of introducing a safe threshold," Nat. Commun. **11**(1), 310 (2020).

[4]Amari, S., Verilhac, J.-M., Gros D'Aillon, E., Ibanez, A., and Zaccaro, J., "Optimization of the growth conditions for high quality $CH_3NH_3PbBr_3$ hybrid perovskite single crystals," *Cryst. Growth Des.* ■, ■ (2020).

[5]D. Shi, V. Adinolfi, R. Comin, M. Yuan, E. Alarousu, A. Buin, Y. Chen, S. Hoogland, A. Rothenberger, K. Katsiev *et al.*, "Low trap-state density and long carrier diffusion in organolead trihalide perovskite single crystals," Science **347**(6221), 519–522 (2015).

[6]W. Wei, Y. Zhang, Q. Xu, H. Wei, Y. Fang, Q. Wang, Y. Deng, T. Li, A. Gruverman, L. Cao *et al.*, "Monolithic integration of hybrid perovskite single crystals with heterogenous substrate for highly sensitive x-ray imaging," Nat. Photonics **11**(5), 315–321 (2017).

[7]H. Wei, Y. Fang, P. Mulligan, W. Chuirazzi, H.-H. Fang, C. Wang, B. R. Ecker, Y. Gao, M. A. Loi, L. Cao *et al.*, "Sensitive x-ray detectors made of methylammonium lead tribromide perovskite single crystals," Nat. Photonics **10**(5), 333–339 (2016).

[8]H. Wei, D. DeSantis, W. Wei, Y. Deng, D. Guo, T. J. Savenije, L. Cao, and J. Huang, "Dopant compensation in alloyed $CH_3NH_3PbBr_{3-x}Cl_x$ perovskite single crystals for gamma-ray spectroscopy," Nat. Mater. **16**(8), 826–833 (2017).

[9]A. Musiienko, P. Moravec, R. Grill, P. Praus, I. Vasylchenko, J. Pekarek, J. Tisdale, K. Ridzonova, E. Belas, L. Landová *et al.*, "Deep levels, charge transport and mixed conductivity in organometallic halide perovskites," Energy Environ. Sci. **12**(4), 1413–1425 (2019).

[10]X. Wang, D. Zhao, Y. Qiu, Y. Huang, Y. Wu, G. Li, Q. Huang, Q. Khan, A. Nathan, W. Lei *et al.*, "PIN diodes array made of perovskite single crystal for x-ray imaging," Phys. Status Solidi RRL **12**(10), 1800380 (2018).

[11]E. Lukosi, T. Smith, J. Tisdale, D. Hamm, C. Seal, B. Hu, and M. Ahmadi, "Methylammonium lead tribromide semiconductors: Ionizing radiation detection and electronic properties," Nucl. Instrum. Methods Phys. Res., Sect. A **927**, 401–406 (2019).

[12]X. Liu, H. Zhang, B. Zhang, J. Dong, W. Jie, and Y. Xu, "Charge transport behavior in solution-grown methylammonium lead tribromide perovskite single crystal using α particles," J. Phys. Chem. C **122**(26), 14355–14361 (2018).

[13]A. Musiienko, J. Pipek, P. Praus, M. Brynza, E. Belas, B. Dryzhakov, M.-H. Du, M. Ahmadi, and R. Grill, *Deciphering the Effect of Traps on the Electronic Charge Transport Properties of Methylammonium Lead Tribromide Perovskites* (■, 2019).

[14]International Standard, ■ (International Electrotechnical Commission, 2003).

AQ3 AQ4 AQ5 AQ6